Chemical Science

Accepted Manuscript

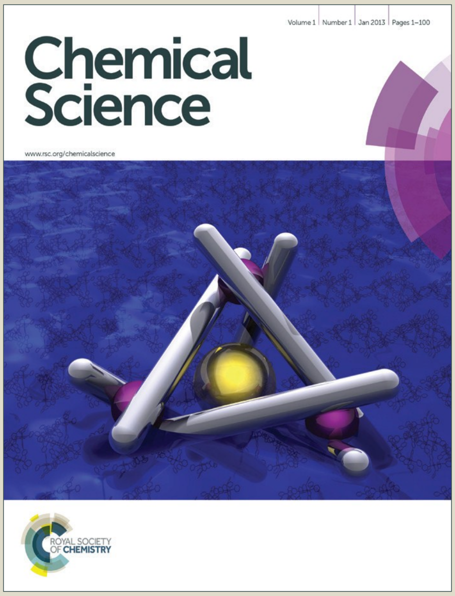

ROYAL SOCIETY OF CHEMISTRY

www.rsc.org/chemicalscience

Chemical Science

EDGE ARTICLE

Interplay between surface chemistry and performance on rutile-type catalysts for halogen production†

Received 00th January 20xx,
Accepted 00th January 20xx

DOI: 10.1039/x0xx00000x

www.rsc.org/chemicalscience

Maximilian Moser,[a] Vladimir Paunović,[a] Zhen Guo,[a] Laszlo Szentmiklósi,[b] Miguel G. Hevia,[c] Michael Higham,[c] Núria López,[c]* Detre Teschner,[d]* and Javier Pérez-Ramírez[a]*

Catalytic HBr oxidation is an integral step in the bromine-mediated functionalisation of alkanes to valuable chemicals. This study establishes the relationships between the mechanism of HBr oxidation over rutile-type oxides (RuO_2, IrO_2, TiO_2) and their apparent catalytic performance. Comparison with the well-studied HCl oxidation revealed distinct differences in surface chemistry between HBr and HCl oxidation that impact the stability and activity of the catalysts. The kinetic fingerprints of both oxidation reactions over the three rutile-type oxides investigated are compared using Temporal Analysis of Products, which substantiate the energy profiles dervied from Density Functional Theory. The quantitative determination of the halogen uptake under *operando* conditions using Prompt-Gamma Activation Analysis demonstrates that RuO_2 suffers from extensive subsurface bromination upon contact with hydrogen bromide, particularly at low temperature and low O_2:HBr ratios, which negatively affects the stability of the catalyst. TiO_2 exhibits intrinsically low halogen coverage (30-50%) at all the conditions investigated due to its unique defect-driven mechanism that renders it active and stable for Br_2 production. On the contrary, in HCl oxidation TiO_2 is inactive and the chlorination of the highly active RuO_2 is limited to the surface. Differences in the extent of surface halogenation of the materials, were also confirmed by High-Resolution Transmission Electron Microscopy and explained by the DFT calculations. These insights into the molecular-level processes taking place under working conditions pave the way to the design of the next generation catalysts for bromine production.

Introduction

The surface chemistry of metal oxides that exhibit a rutile structure is rich and complex.[1] Their dense lattice structure renders these materials stable against harsh reaction conditions and make them an attractive option for applications in heterogeneous, electro, and photo catalysis.[1,2] Recently, the implementation of RuO_2-based catalysts for the recovery chlorine *via* the oxidation of HCl, a copious by-product of the polyurethane and polycarbonate production, stimulated multiple studies employing interdisciplinary methods.[1,3] It was demonstrated that the stability of RuO_2 against bulk chlorination originates from a self-limiting mechanism that confines the chlorination to the surface, while its low temperature activity is linked to the small energetic barrier for the evolution of chlorine.[4] *Operando* studies on RuO_2 showed that the activity is related to its extent of surface chlorination and can be controlled through variation of temperature and oxygen partial pressure.[5]

Rutile-type catalysts were also studied for the gas-phase oxidation of HBr to Br_2; a crucial step to close the bromine cycle in emerging bromine-mediated alkane functionalisation processes.[6] It was found that RuO_2- and IrO_2-based systems catalyse the HBr oxidation at much lower temperatures than the HCl oxidation due to the lower energy barrier of the bromine evolution compare to that of chlorine.[6d] Further studies resulted in the discovery of TiO_2 as an active catalyst for HBr oxidation, despite its inertness in HCl oxidation.[7] Molecular modelling proposed that a self-doping mechanism with bromine enables the adsorption and activation of molecular oxygen on TiO_2.[7] These results underlined that the mechanism of HBr oxidation is more multifarious than that of HCl oxidation on rutile surfaces. However, there is a lack of systematic studies enabling one to rationalise the relationship between the state of the surface and the apparent catalytic performance over different rutile-type catalysts in HBr oxidation. A comprehensive mechanistic picture can be developed through a multidisciplinary approach combining theoretical calculations with *ex situ* and *operando* methods.

---

[a] *Institute for Chemical and Bioengineering, Department of Chemistry and Applied Biosciences, ETH Zurich, Vladimir-Prelog-Weg 1, 8093 Zurich, Switzerland.*

[b] *Centre for Energy Research, Hungarian Academy of Sciences, Konkoly-Thege Miklós street 29-33, 1121 Budapest, Hungary.*

[c] *Institute of Chemical Research of Catalonia, ICIQ, Barcelona Institute of Science and Technology, BIST, Av. Països Catalans 16, 43007 Tarragona, Spain.*

[d] *Fritz-Haber-Institute of the Max Planck Society, Faradayweg 4-6, 14195 Berlin, Germany.*

* *E-mails: nlopez@iciq.es (N.L.), teschner@fhi.mpg.de (D.T.), jpr@chem.ethz.ch (J.P.-R.)*

† Electronic Supplementary Information (ESI) available: Additional Computational details, additional HRTEM analysis, energy values, illustrations, and contour plots of the ab initio thermodynamics, transient responses of TAP experiments, reaction profile of the HX oxidation half cycle, rate of halogen formation versus the halogen coverage. See DOI: 10.1039/x0xx00000x

Herein, we undertake a detailed study of the surface chemistry of rutile-type catalysts, *i.e.* RuO_2, IrO_2, and TiO_2 in HBr oxidation including a direct comparison to HCl oxidation. Advanced characterisation techniques provide an in-depth perspective on the catalytic hydrogen halide oxidation that goes beyond the experimental limitations of previous studies on HBr oxidation. Analysis of microscopic imaging and energy profiles calculated from Density Functional Theory rationalise the interaction of the gas environment with the catalysts. The dynamics of product formation are deduced from Temporal Analysis of Products. These are combined with *operando* Prompt Gamma Activation Analysis experiments under steady-state conditions, enabling the determination of the halogen surface coverage. Combining these results, we discuss the impact of surface halogenation by hydrogen halides on the structural stability of the rutile materials and the mechanistic fingerprints of the hydrogen halide oxidation over these catalysts.

Experimental

Catalyst preparation. The as-received RuO_2 (11 $m^2\ g^{-1}$, Aldrich, 99.5%) and TiO_2 (20 $m^2\ g^{-1}$, Aldrich, rutile nanopowder, 99.5%) powders were calcined at 723 and 823 K, respectively, using a ramp of 5 K min^{-1} and a holding time of 5 h. IrO_2, (9 $m^2\ g^{-1}$) was prepared by calcination of anhydrous $IrCl_3$ (ABCR, 99.9%) at 823 K for 5 h using a heating rate of 5 K min^{-1}.

High-resolution transmission microscopy. High-Resolution Transmission Electron Microscopy (HRTEM) was undertaken either in a FEI Tecnai F30 microscope operated at 300 kV or in a FEI Talos microscope operated at 200 kV. Elemental mapping using Energy-Dispersive X-ray Spectroscopy (EDXS) was measured in STEM-mode with 4 X-rays detectors (Bruker) attached to the Talos microscope. Prior to microscopic analysis, the solids were dispersed in ethanol; a few droplets of the suspension were poured onto a holey carbon-coated copper grid and dried completely.

Computational details. Density Functional Theory (DFT), as implemented in the Vienna *Ab initio* Simulation Package (VASP) version 5.3.3, was applied to slabs representing the rutile (110) facet, for both RuO_2 and TiO_2.[8] For all rutile-type catalysts the (110) surface represents the largest contribution to the surface in the Wulff construction of the nanoparticles. For example, RuO_2 exhibits 43% of the (110) facet and a complementary 42% of the (101) facet.[5b] For calculations involving RuO_2(110), a $p(2\times1)$ supercell was employed, with a k-point sampling of 4×4×1, using the scheme of Monkhorst and Pack.[9] For calculations involving TiO_2(110), the chosen slab corresponds to a $p(2\times2)$ supercell, with a k-point sampling of 4×2×1. In both cases, slabs consisting of five layers were interleaved by 15 Å of vacuum. The top two layers of the slabs were optimised, while the remaining bottom three were fixed. Forces were converged to within 0.015 eV $Å^{-1}$. In order to eliminate the spurious electrostatic interactions associated with asymmetric relaxation of the slab, a dipole correction was applied to the vacuum. The exchange-correlation functional PBE,[10] as well as PBE+U[11] for TiO_2, was employed, with U_{eff} = 4.5 eV for Ti. Inner electrons were replaced with PAW,[12] and the valance states were expanded in plane-waves with a cut-off energy of 450 eV. Spin-polarised calculations were performed as necessary. Transition states were identified by CI-NEB.[13] *Ab initio* thermodynamics were performed using lowest energy surface configurations to determine the surface composition under typical experimental conditions as a function of the partial pressures $p(HX)$, $p(H_2O)$, and $p(X_2)$; (X = Cl, Br). The experimental gas-phase thermodynamic data from the NIST reference tables were utilised in conjunction with DFT results for the relevant molecular species (*viz.* HCl, HBr, Cl_2, Br_2, and H_2O).[14] The simulations were conducted under various partial pressures and temperatures over RuO_2 and TiO_2 with different degrees of halogenation. Additional computational details with regard to halogen substitution in the rutile structures are provided in the Electronic Supplementary Information. Notice, that the results of the *ab initio* thermodynamics indicate the most stable configuration of the material as a function of external temperatures and pressures. Thus, the lowest energy halide distributions are identified, but not the process (kinetics or mechanism) of how subsurface halide uptake takes place.

Temporal analysis of productions. Transient mechanistic studies of HBr and HCl oxidation over RuO_2, IrO_2, and TiO_2 were carried out in a TAP-2 reactor.[15] The samples (10 mg, particle size = 0.2-0.4 mm) were loaded in the isothermal (central) zone of a stainless steel micro-reactor (4.6 mm internal diameter) between two layers of quartz particles of 0.125-0.2 mm. The thickness of the catalyst zone (1-2 mm) was very small compared with the overall bed length (37 mm). This configuration, referred to as thin-zone reactor, is characterised by negligible gas concentration gradients across the catalyst bed.[15b] The samples were pre-treated in a flow of 20 cm^3 STP min^{-1} O_2 at 623 K and 1 bar for 1 h, followed by evacuation of the reactor to 10^{-10} bar. The following pulse experiments were carried out in high vacuum at 523, 573, and 623 K for HBr and at 623 K for HCl oxidation, using a pulse size of *ca.* 10^{16} molecules: (a) Individual pulsing of either O_2:He = 8:1 or HX:Ar = 16:1 (X = Cl, Br); (b) Simultaneous pulsing of O_2:He = 8:1 and HX:Ar = 16:1; (c) Pump-probe pulsing of O_2:He = 8:1 and HX:Ar = 4:1. The latter are also referred to as sequential pulsing, where the pulses of the two gas mixtures are separated by a time delay (Δt). The pulses were separated by 0.25 and 1 s for O_2:He (pump pulse) and HX:Ar (probe pulse). In the case of HX:Ar (pump pulse) and O_2:He (probe pulse), the delays were 2 and 8 s. The pump and probe pulses were repeated cyclically, keeping a time interval of 8 s between the probe pulse in one cycle and the pump pulse in the following cycle constant in all cases.

In the experiments, Ar (Linde, purity 5.0), He (Air Products, purity 5.2), O_2 (Air Products, purity 5.2), HBr (Linde, purity 4.5), and HCl (Linde, purity 2.8) were used. A quadrupole mass spectrometer (RGA 300, Stanford Research Systems) monitored the transient responses at the reactor outlet of the following atomic mass units (AMUs): 160 (Br_2), 80 (HBr), 70

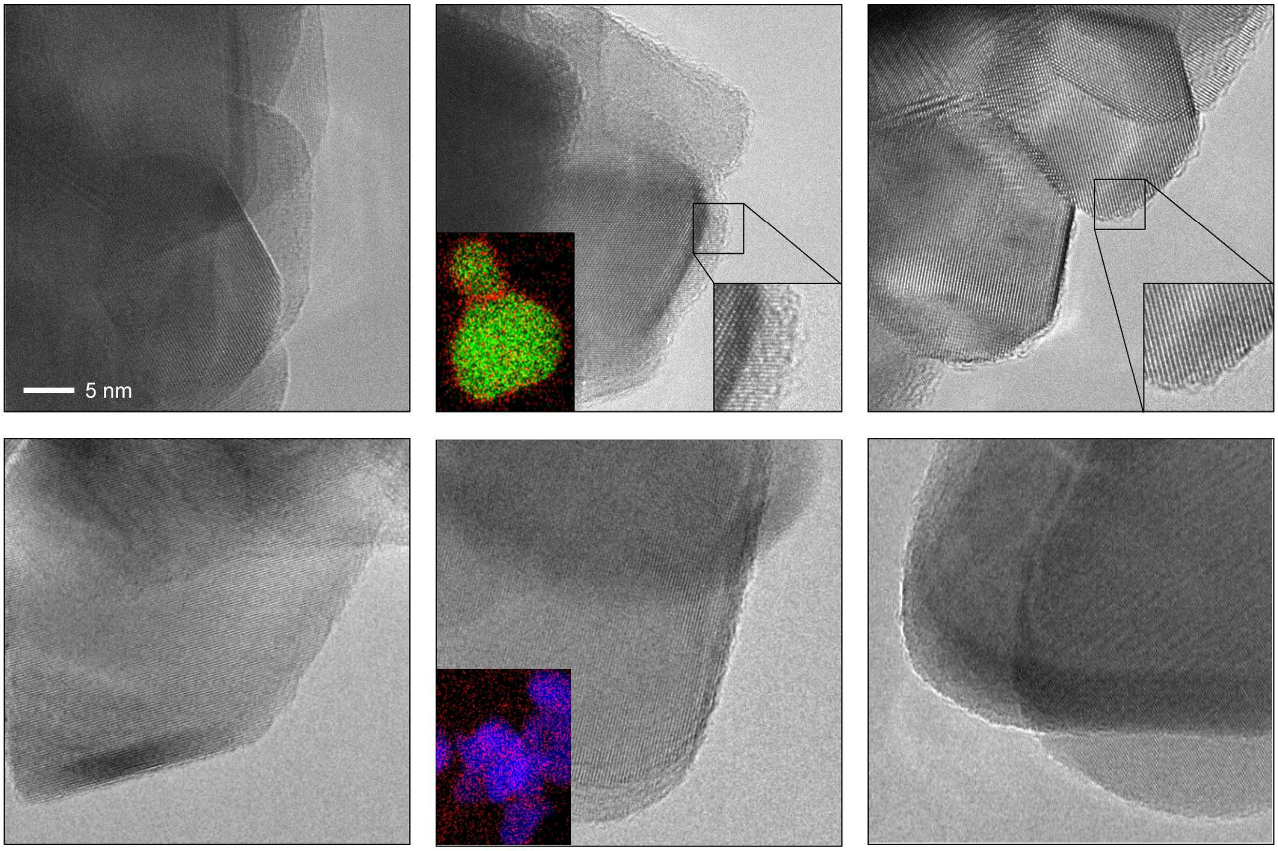

Fig. 1. HRTEM of RuO_2 (top) and TiO_2 (bottom) showing the as-prepared materials (left), after treatment in HBr at 393 K (centre), and HCl at 543 K (right). The scale bar in the top left image applies to all. The bottom left insets in the centre micrographs depict the averaged elemental mapping of the RuO_2 and TiO_2 particles using EDXS with Ru (green), Ti (blue) and Br (red). The bottom-right insets in the top centre and right micrographs show a magnification of the amorphised particle edges. Additional micrographs of RuO_2 and TiO_2 (Figs. S1, S2) and structural models (Fig. S4, S5) of brominated RuO_2 are provided in the Electronic Supplementary Information.

(Cl_2), 40 (Ar), 36 (HCl), 32 (O_2), 18 (H_2O), and 4 (He). The responses displayed correspond to an average of 20 pulses per AMU to improve the signal-to-noise ratio. Prior to that, it was verified that the responses were stable; that is, with invariable intensity and shape during at least 40 consecutive pulses.

Operando prompt gamma activation analysis. The Br and Cl uptake on the rutile-type catalysts during HBr and HCl oxidation was determined using *operando* Prompt Gamma Activation Analysis (PGAA) at the cold neutron beam at the Budapest Neutron Centre. The technique was successfully used to study the surface chlorination of Deacon catalysts[5,16] and is based on the neutron capture of the atomic cores in the sample and the subsequent detection of element-specific gamma rays emitted during de-excitation of the nuclei. The gas-phase oxidation of hydrogen halides was studied in a quartz fixed-bed micro-reactor (8 mm internal diameter) at ambient pressure and in the temperature range of 413-713 K. The reactor was loaded with 0.5 g of RuO_2 or 0.23 g of TiO_2 catalyst (particle size = 0.4-0.6 mm) and was placed inside a furnace in the path of the neutron beam. A total volumetric flow of 250 cm^3 STP min^{-1} consisting of 10 vol.% HBr or HCl (Air Liquide, anhydrous) and 0-90 vol.% O_2 (Linde, purity 4.5) balanced in N_2 (Linde, purity 5.0) was continuously fed. Furthermore, 0-4 vol.% Br_2 (Acros, 99.8%) were added to the gas feed by passing a split of the N_2 flow through a saturator filled with liquid Br_2 at STP conditions. The halogen formation was quantified by iodometric titration using a Mettler Toledo G20 Compact Titrator as detailed elsewhere.[4d] The rate of halogen formation was expressed as mole of halogen produced per gram of catalyst and unit of time. The cold neutrons were guided to the experimental station by curved supermirror neutron guides. A Compton-suppressed high-purity germanium (HPGe) crystal detects the prompt gamma photons emitted by the catalyst bed. Br, Cl, Ru, and Ti were determined from the characteristic peak areas. The surface coverage was calculated as the amount of halogen per surface sites taking into account the surface area of the catalysts and the density of sites of the (110) and (101) facets weighted by their relative occurrence.[5a,17] The gas-phase signals of HBr, Br_2, HCl, and Cl_2 were subtracted, thus, all reported values correspond only to the solid catalyst.

Results and discussion

Halogenation of rutile structures. The as-prepared RuO_2 and TiO_2 samples exhibited nanoparticles with diameters of *ca.* 20 nm and 50 mm, respectively, and sharp edges with clearly visible fringes, providing for a high degree of crystallinity as shown by HRTEM (Fig. 1). After treatment in both HBr and HCl for 3 h (*i.e.* O_2:HX = 0), both RuO_2 and TiO_2 particles retain their size, while the RuO_2 surfaces exhibit significant amorphisation compared to TiO_2. The evaluation of the RuO_2 crystals shows that the amorphised layer is thicker after treatment in HBr compared to HCl (Figs. 1, S1). The analysis of the HBr-treated samples with EDXS corroborates this observation, detecting a significant concentration of bromine along the particle edges (Fig. 1, middle). The TiO_2 surfaces are virtually unaffected by the HBr and HCl treatment. The EDXS mapping of TiO_2 did not detect significant traces of chlorine and only small amounts of bromine (Fig. 1, S2). These results are further supported by the measured halogen uptake under reaction conditions, which indicate a four times higher bromine uptake compared to chlorine on RuO_2 and comparably low halogen uptake on TiO_2 *(vide infra)*.

In previous studies, it has been observed that rutile-type catalysts used in heterogeneous catalysis are affected by the chemical environment under which the reaction takes place. The theoretical investigation of the active phase can be conducted at different levels of complexity. For instance, bulk stability against complete halogenation (*i.e.* where bulk MO_2 is replaced by MX_n), and the possibility of rutile degradation *via* the formation of volatile species: ($TiCl_4$ formation would be an example) could also be considered. However, to address the formation of mixed phases it is more illustrative to conduct simulations of the substitution of surface and subsurface oxygen atoms by halogen atoms in the lattice of RuO_2. The theoretical replacement energies reported were calculated according to the equation $RuO_2 + 2nHX \rightarrow RuO_{2-n}@X_n + nH_2O + n/2X_2$, where n is the number of oxygen atoms replaced and X refers to either Br or Cl. Lattice oxygen is evolved to the gas phase in the form of water. The energies for RuO_2 bromination are most exothermic for configurations corresponding to the substitution of two O atoms ($\Delta E_r = -1.97$ eV, Fig. S3, 2A), and remained significantly exothermic for up to four Br atoms ($\Delta E_r > -1$ eV, Fig. S3, 4B). Upon the addition the first subsurface Br atom, the bromination becomes less exothermic ($\Delta E_r = -0.50$ eV, Fig. S3, 5C) and eventually it is slightly endothermic after the addition of a further Br atom ($\Delta E_r = 0.30$ eV, Fig. S3, 6H). Notably, the incorporation of four or more Br atoms into the cell already leads to a considerable degree of structural rearrangement (Fig. S4, 4B, 4F). The surface Br atoms relax such that they form a hexagonal arrangement (Fig. S5). The high Br density of these structures presents a change in the geometry that would appear as amorphisation in the experiments (Figs. 1, S1). Furthermore, considering factors unaccounted by the above methodology, such as configurational entropy or other surface orientations, extensive subsurface bromination is well within the bounds of possibility.[4c] The present calculations only aim at establishing the lowest energy configurations and do not provide any indication as to how the bromination occurs. For RuO_2 chlorination, the process is only exothermic for up to two Cl atoms incorporated into the surface ($\Delta E_r = -0.93$ eV, Fig. S3, 2A), with subsequent Cl addition being endothermic (Fig. S3b, 3A). While incorporation of up to four Cl atoms is moderately endothermic ($\Delta E_r = 0.71$ eV, Fig. S3, 4B), subsequent chlorination to subsurface layers is considerably more so, reaching $\Delta E_r = 1.81$ eV and 3.21 eV, for five and six Cl atoms, respectively (Fig. S3, 5C, 6H).

Ab initio thermodynamics studies were performed to identify which halogenated structures would be stable under the treatment conditions, *i.e.* variable HX and low product partial pressures (Fig. 2).[‡] The results show, that the surface composition consists of between two to four Br or two Cl atoms per (2x1) between $p(HX) = 10^{-2}$ and 100 bar.[§] Higher $p(HX)$ favour more extensively halogenated structures, while the free energy for substitution of Br atoms remains more exothermic than that for Cl for all partial pressures in the range considered. This indicates that bromination is stronger under comparable conditions, as observed in the microscopic analysis. The impact of $p(H_2O)$ and $p(X_2)$ on the RuO_2 surface composition is less pronounced (Figs. S6, S7), with the surface structure showing considerably less variation over the same

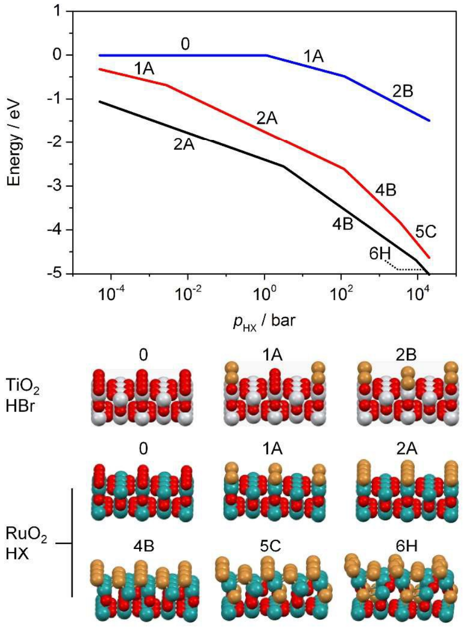

Fig. 2. Free energy of substitution *versus* the partial pressure of the hydrogen halide for the bromination of TiO_2 (blue) and RuO_2 (black), as well as for the chlorination of RuO_2 (red). The partial pressures of X_2 and H_2O were fixed at 10^{-4} bar. The temperature was set to 573 K (TiO_2) and 393 K (RuO_2) for bromination and 523 K (RuO_2) for chlorination. The labels in the plot correspond to the structures shown below, which exhibit the lowest free energy under the simulated conditions. These depict the substitution of Cl or Br atoms into the surface and subsurface layers. Colour code: Ti (grey), Ru (blue), O (red), and Cl or Br (brown).

pressure range as compared to p(HX).

The calculations for TiO_2, on the other hand, show that Br uptake is endothermic for both one and two Br atoms incorporated with ΔE_r = 0.43 eV and 1.33 eV, respectively (Fig. S8, 1A, 2B). The lowest energy configuration for two Br atoms had them both occupying bridging sites in diagonal fashion, as this would result in minimal repulsion between them (Fig. S8a, 2B). Our *ab initio* thermodynamics suggest that under typical experimental conditions, *i.e.* low $p(H_2O)$, and $p(Br_2)$, as well as high p(HBr), the Br uptake is limited, with a maximum of one Br atom per (2×2) surface cell. Furthermore, the free energy of substitution of a Br atom into TiO_2 is much lower than for both RuO_2 chlorination and bromination (Fig. 2). The product partial pressures have a very limited impact on the surface bromination, thus indicating that the HX partial pressure is the dominant factor in determining the halogenation of rutile-type structures.

Mechanistic studies. The analysis of the reaction mechanism of HBr and HCl oxidation was conducted by combining pulse experiments in a TAP-2 reactor with DFT calculations, which allowed us to study the reactant and product evolution corroborated by molecular simulations. In order to compare the interaction of HBr and HCl with the catalysts, individual pulses of either HBr or HCl molecules were applied to the rutile catalysts (Fig. 3). When comparing the normalised peak responses of HCl and HBr, we observe that the HBr peaks are significantly delayed compared to the HCl peaks by 0.44 s (RuO_2), 0.82 s (TiO_2), and 0.17 s (IrO_2). This indicates a stronger interaction of HBr with the surface than HCl, which is in line with the HRTEM and DFT results, and the calculated dissociative adsorption energy over $RuO_2(110)$, which is −2.33 eV for HBr compared to −2.09 eV for HCl on the clean surface. Comparing the catalysts, the order of the HBr peak maxima is as follows: $RuO_2 < IrO_2 < TiO_2$ at 523, 573, as well as 623 K (Fig. S9). The peak position is affected by changing the temperature, showing a significant delay of the peak time at higher temperature. This indicates a sizable activation barrier in the overall process during TAP experiment, which is likely due to underlying surface/sub-surface processes (*vide supra*). Furthermore, a shift between the HBr pulses of individual HBr and simultaneous HBr+O_2 pulsing is observed for IrO_2 (0.31 s), and TiO_2 (0.67 s) (Fig. 3). The shift could be due to the reaction of HX and O_2 to X_2 and water, where the reactants are consumed (Figs. 3, S10), leading to a reduction of the integrated peak area. This leads to a shift of the HX peak maximum to shorter times and less tailing of the signal in comparison to the individual pulsed reactant signal assuming that the pulse size of reactant was about the same in both individual and simultaneous pulsing experiments.[4d,18] For RuO_2 a difference in tailing is observed, but no clear shift of the peak position is visible, which might indicate that the interaction between RuO_2 and HBr is not significantly affected by the simultaneously pulsed oxygen. For HCl oxidation, only RuO_2 exhibits a clearly narrower tailing of the HCl response when comparing individual HCl and simultaneous HCl+O_2 pulses, indicating that only RuO_2 is significantly active under TAP conditions (Fig. S10). Thus, only RuO_2 is considered for further comparative evaluation of HBr with HCl oxidation. The comparison of the O_2 pulses after individual O_2 and simultaneous HBr+O_2 pulsing does not show a clear difference, because the integrated peak area is generally 10 times higher (Fig. S10). This further indicates the presence of state-defining conditions as the oxidic surface seems to be unchanged upon admitting the large O_2 pulses.[15d] In addition, the halogen surface coverage can be assumed to be very low (*i.e.* < 1%), due to the small size of the HX gas pulses compared to the total surface area of the loaded catalysts under UHV conditions. Thus, extensive surface or subsurface halogenation of the catalysts does not occur.

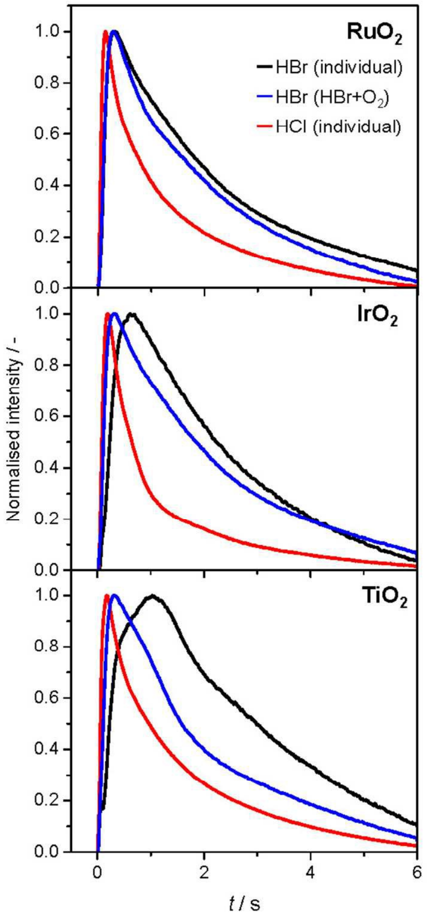

Fig. 3. Normalised transient responses of HBr and HCl after individual (HBr, black; HCl, red), and simultaneous (HBr+O_2, blue) pulse experiments at 623 K.

The product responses of Br_2, Cl_2, and H_2O after simultaneous pulsing of O_2 with either HCl or HBr are depicted in Fig. 4. When comparing the product responses, it is evident that Cl_2 production is greater than Br_2 production over RuO_2 at the same temperature, which could be explained by the very low detection efficiency of the Br_2 molecules by the mass spectrometer, due to the lower bond strength of Br_2

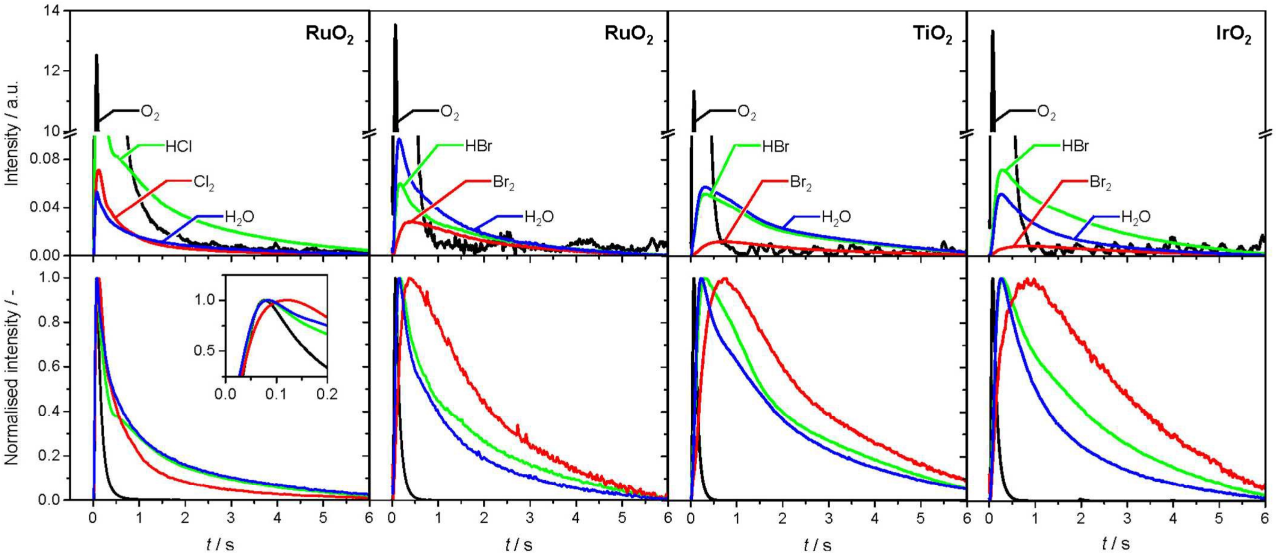

Fig. 4. Transient (top) and normalised transient (bottom) responses of reactants (HCl, HBr, O_2) and products (Br_2, Cl_2, H_2O) at 623 K upon simultaneous pulsing of HX and O_2 over rutile-type catalysts. The colour code applies to both the top and bottom rows. The break in the y-axis in the top plots enables a better visualization of the product responses: Cl_2, Br_2, and H_2O. The inset in the bottom left plot magnifies the region at the maximum of the normalised transient responses.

(193 kJ mol^{-1}) in comparison with the Cl_2 (243 kJ mol^{-1}) preventing a direct comparison of their signals. The bond strength of HBr (363 kJ mol^{-1}) and HCl (428 kJ mol^{-1}) is comparably high so no effect on the detection efficiency is assumed. The direct calibration of QMS using pulses of bromine and chlorine has been considered, but was not conducted due to the unjustifiable damage expected to occur due to corrosion. However, comparing the water signal, which forms in stoichiometric amounts to either Br_2 or Cl_2, indicates that the rate of bromine formation must be higher than the chlorine formation. The pulse response size of the water and bromine signals increases in the order: $IrO_2 < TiO_2 < RuO_2$ indicating the higher activity (Fig. 4, top row). The normalised signals show that the water response always reaches its peak maximum before the halogen, suggesting that the halogen evolution is slower and can be considered the most-energy demanding step (Fig. 4, bottom row). However, the differences in mass between water and the halogen molecules could affect the observed shift of the peak response in the molecular diffusion regime, hampering in particular the comparison of water to chlorine responses due to their small difference. In case of HBr oxidation, the shift between the HBr and Br_2 peak maximum can be safely interpreted as a measure for the activity of the catalysts. The shifts decrease in the order IrO_2 (0.60 s) < TiO_2 (0.43 s) < RuO_2 (0.22 s), which coincides with the product formation in the opposite order.

The observed faster bromine evolution over TiO_2 compared to IrO_2 is a crucial piece of experimental evidence reaffirming the computational results. This proof could not be delivered by atmospheric pressure steady-state experiments because the apparent activity of both oxides in HBr oxidation was very similar. This is likely due to a compensation effect similar to that, which occurs in the Deacon reaction on RuO_2 at high coverage.[5a] The compensation that occurs between both materials is proposed to result from a breaking of the scaling relationships, as discussed recently.[7] In the present work, the pulsing experiments in TAP allow the elementary steps of the reaction network to be decoupled. In this sense, it is possible to investigate only the desorption process as it occurs under very low coverage and state-defining conditions as explained above. Thus, in the absence of high bromine coverage we were able to observe the intrinsic differences in bromine evolution between TiO_2 and IrO_2 as postulated in reference 7.

In order to verify the reaction mechanism of the HBr and HCl oxidation, pump-probe experiments were conducted, where either the HX or the O_2 pulse was delayed by a distinct time period (Figs. S11, S12). In the O_2 (pump) and HX (probe) pulsing experiment, product formation can be observed after either pulse. The product formation after the HX probe pulse is much larger, which is due to the available oxygen on the surface following the pump pulse (Fig. S11). This is analogous to the HX (pump) and O_2 (probe) pulsing, where the product formation after the HX pump pulse is also significant. The large product formation after O_2 can be related to oxygen-assisted product evolution (Fig. S12), as described for HCl oxidation in recent studies.[5a]

To further interpret our experiments and to complement earlier results,[7] we computed the reaction profiles for the HBr and HCl oxidation over halogenated rutile surfaces (Fig. S13). For better comparison, the most important reaction steps are depicted in Fig. 5. The basic surface sites can strip a proton from HX, resulting in a surface hydroxyl and an adsorbed halide ion. Re-oxidation was identified as the key step in Deacon catalysis on RuO_2 to close the cycle; this is the step where most differences appear between RuO_2 and TiO_2. O_2 adsorption on metallic surfaces like RuO_2 and IrO_2 is limited

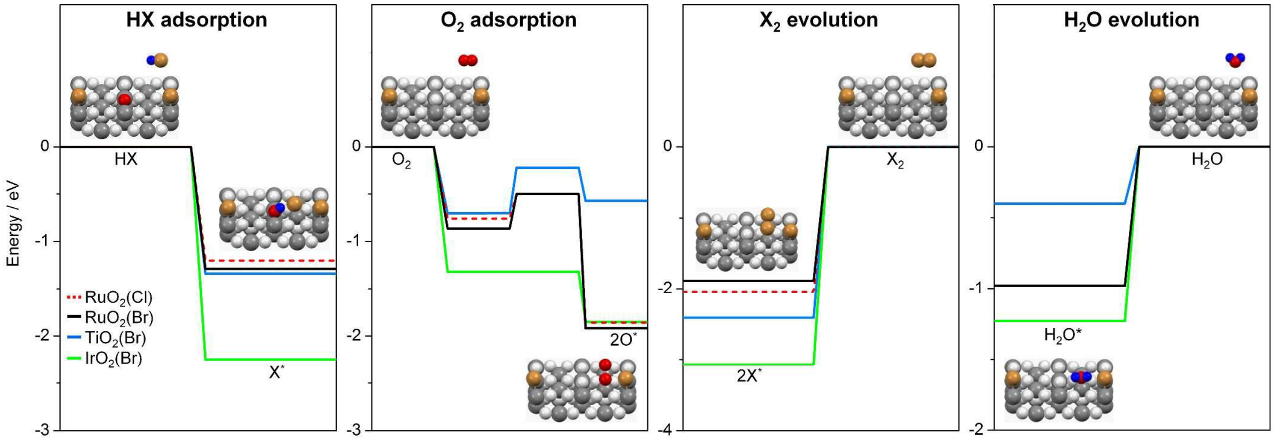

Fig. 5. Key steps of reactant adsorption and product evolution steps for HBr (solid lines) and HCl (dashed line) oxidation on halogenated rutile-type surfaces. The H_2O evolution step for RuO_2(X) in HBr (black) and HCl (red) oxidation overlap. The full reaction profile is shown in Fig. S13. The inserts illustrate the reaction steps on a rutile surface. Colour code: Metal atom (dark grey), Br (brown), H (blue), and O (light grey and red). O atoms are coloured in red, if they participate in the reaction.

only by the number of free active sites available on the surface.[19] On TiO_2, oxygen chemistry is necessarily related to defect chemistry.[7] In the present case, the defect chemistry originates from one of the reactants (HBr), so it can be partially understood as auto-catalytic. This activity is only possible for HBr; as the Cl (3*p*) levels in Cl are far too low in energy compared to the Br (4*p*) levels in Br (resulting in a stronger adsorption for Cl), and thus the energy required to eliminate Cl_2 from the surface is far too high for the reaction to occur in the temperature window for TiO_2 activity.[7] In addition, for the HX oxidation to take place, sites capable of both acid-base and redox interactions are required.[7] Metal oxides with metallic properties exhibit both of these characteristics to a reasonable degree, but redox properties are more subtle for semiconductors, where defect levels play the leading role. In view of the product evolution, Cl_2 recombination is more energy demanding than Br_2, with recombination energy of the latter over different surfaces increasing in the following order: RuO_2(Br) (1.9 eV) < TiO_2(Br) (2.44 eV) < IrO_2(Br) (3.05 eV).[§§,20] This coincides with the product evolution from the simultaneous pulsing experiments. The recombination of two halide atoms on the surface is the most energy-demanding reaction step in all investigated systems. Water evolution is less energy demanding by more than 1 eV (Fig. 5). For the latter, the hydroxyl groups can recombine over the surface, generating an adsorbed water molecule that can then leave the surface. These water-related steps are very similar in their mechanism on all of the surfaces.

Impact of the halogen surface coverage. The halogen coverage on the catalysts was determined by *operando* PGAA under real-life conditions on RuO_2 and TiO_2. An investigation of IrO_2 was unfortunately not possible, because the neutron excitation and radioactive decay of Ir leads to the emission of very intense gamma radiation that rapidly saturates the detector, and the high baseline created by the Ir matrix overshadows the Br signal.[21] Thus, the comparison focused on TiO_2 and RuO_2 at variable O_2:HX feed ratios and temperatures (Fig. 6), where the HCl and HBr conversion reached maximum values of 29% and 84%, respectively.

As shown in Fig. 6a, TiO_2 exhibits halogen coverages of 0.57 and 0.48, for Br and Cl respectively, at O_2:HX = 0. With increasing oxygen partial pressure these values decrease to 0.4 (Br) and 0.36 (Cl). The Cl coverage on RuO_2 is close to 1 at O_2:HCl = 0 and reaches 0.86 at O_2:HCl = 9, which is in line with recent studies.[5] However, in agreement with our HRTEM and DFT results, RuO_2 exhibits subsurface bromination when conducting the same O_2:HBr ratio variation from 0 to 9, reaching a degree of bromination that exceeds the theoretical full surface coverage by 300% (Fig. S14). Therefore, the tests on RuO_2 in HBr were conducted under slightly different conditions, with the O_2:HBr ratio decreasing from 9 to 1, whereby the Br coverage increased from 0.65 to 1.48, respectively (Fig. 6a). The dependence of the halogen coverage on the variation of the bed temperature, as indicated in the respective plots, is very similar to that of the oxygen partial pressure (Figs. 6b, S15). By increasing the temperature the halogen coverage on TiO_2 drops from 0.41 (Br) and 0.54 (Cl) to 0.27 (Br) and 0.38 (Cl), respectively. The halogen coverages on TiO_2 are significantly lower compared to RuO_2, which is in agreement with the ab initio thermodynamics. In Fig. 6c, data points from the different experiments are combined to show the effect of bromine coverage on the rate under the same reaction conditions. The bromine coverage on TiO_2 is so low that a slight increase in surface bromine content leads to a higher activity. On the other hand, the bromine coverage on RuO_2 is above the theoretical surface coverage and further increases are detrimental to the activity of RuO_2 in HBr oxidation (Fig. 6c). Thus, an optimal halogen coverage between the observed values for TiO_2 and RuO_2 at which the bromine formation rate would be maximal is likely to exist.

The impact of the product inhibition was investigated on TiO_2 by adding bromine to the gas feed (Fig. 7a). The addition of

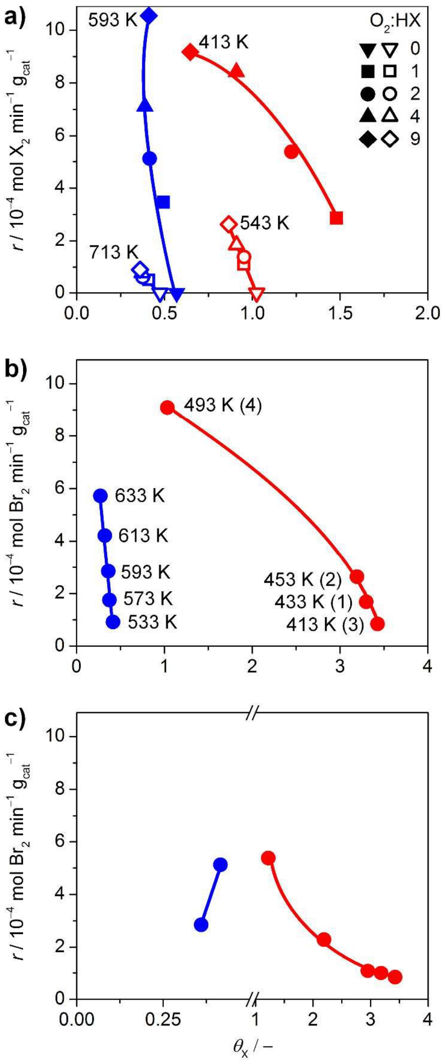

Fig. 6. Rate of halogen formation of HBr (solid symbols) and HCl (open symbols) oxidation as a function of the halogen coverage over TiO_2 (blue) and RuO_2 (red) showing the dependence on the feed O_2:HX ratio at constant temperature (a). The O_2:HX ratio was increased from 0 to 9, except for the HBr oxidation over RuO_2 where the order was inverted from 9 to 1. Dependence of the rate on the catalyst bed temperature at O_2:HBr = 2. The temperature for TiO_2 was increased from 533 K to 633 K (b). The order of measurements for RuO_2 is indicated with numbers in parenthesis. Rate of bromine formation versus the bromine coverage (c). The data points (O_2:HBr = 2, 593 K for TiO_2, and 413 K for RuO_2) are taken for the measurements shown in Figs. 6a, b, and S14. Coverages exceeding unity indicate the occurrence of subsurface halogenation.

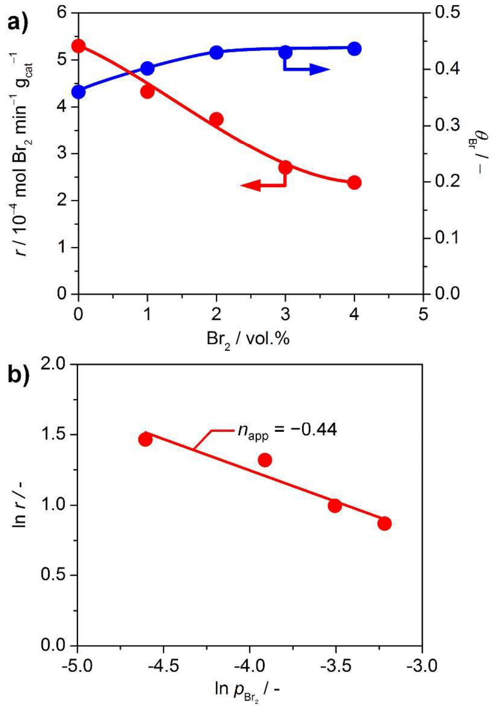

Fig. 7. Rate of bromine formation (red) and bromine surface coverage (blue) versus the volumetric feed of bromine over TiO_2 at 593 K and O_2:HBr = 2 (a). Rate of bromine formation versus partial pressure of bromine (b).

4 vol.% Br_2 causes a distinct decrease in the bromine formation rate by 55%. However, the bromine coverage stabilises at 0.43 after increasing the bromine feed to 2 vol.%. This indicates that there is no significant bromination of the catalysts through the addition of bromine gas, which is in agreement with the endothermic adsorption of Br_2 on clean TiO_2 calculated by DFT (0.69 eV with respect to 1/2 Br_2); a bifunctional adsorption as proposed by Li and Metiu[20] does not improve the adsorption energy. Recent studies highlighted that the gas-phase thermodynamic equilibrium of the HBr oxidation is shifted far to the side of products.[6d] Thus, the decreased activity is not linked to a shift in the thermodynamic equilibrium, but is due to the reaction kinetics. The determination of the apparent reaction order gives a value of −0.44 for the impact of bromine on the reaction rate (Fig. 7b). This value is close the theoretical apparent order of −0.5, which describes the dissociative adsorption of bromine on the active site. Hence, it seems plausible that a competitive adsorption between HBr and Br_2 occurs on the small number of active sites of TiO_2 and likely depends on the defective states left on its surface, originating from doping by the small amount of Br taken up by the surface. To compare, the inhibition effect of Cl_2 on RuO_2 in the Deacon reaction is −1.00.[5a] The larger inhibitions induced on RuO_2 catalysts are due to the fact that site competition is favoured on metallic substrates compared to semiconductors like TiO_2. The ultimate reason for this is that once doped, the Ti centres are no longer chemically equivalent to each other, and thus they discriminate between the adsorption of electron-rich and electron-poor fragments. In comparison, the conduction band in metals screens out these effects, and it is not possible to differentiate the chemical nature of the cations.

Halogen chemistry on rutile surfaces. With all the data described in the previous sections a generalised picture of the chemistry of halogens on rutile catalyst emerges. Although the chemical nature of HCl and HBr might appear to be virtually identical at a first glance, the interaction with the set of potential catalysts is markedly different. Initially, the surface basicity and the acidic character of HX leads to an exothermic adsorption pattern for all combinations. But depending on the particular oxide/hydrogen halide pair, the adsorption can only lead to: (i) a minor fraction of the oxygen lattice replacement (TiO_2/HBr), (ii) a medium level of oxygen lattice replacement and a large surface coverage (RuO_2/HCl) or (iii) an extensive surface modification with concomitant subsurface occupation and the growth of a second phase on the surface (RuO_2/HBr). The factors controlling these differences are related to: (i) the nature of the oxides and (ii) their limited ability to store extra electrons in defect states (TiO_2), while (iii) for the metallic oxides (RuO_2 and IrO_2), the extension of the halide replacement is mostly governed by the relative energies of the M-O and M-X bonds.

The activity of the rutile is then completely governed by the halide content in the material; to quote Paracelsus, the dose makes the poison. Thus, the mechanism might range from only involving surface positions (Langmuir-Hinshelwood-type mechanism), as for HBr on TiO_2, through a continuum that involves the activation and or replacement of surface lattice oxygen atoms (*i.e.* closer to a Mars-van-Krevelen-type mechanism). The active catalyst must then be obtained through the control of the oxygen pressures in the gas-phase that can limit the halide content only to surface positions, thus rendering the catalyst active. The single exception to this behaviour is the semiconductor TiO_2 material. For TiO_2, the self-doping occurring as a result of replacement of the surface oxygen atoms by halide is self-limited due to the energy cost of accumulating electrons in surface and subsurface states.[22] The activity is then linked to the presence of forbidden energy areas from where it is possible to add/extract electrons and how effective the alignment of the energy levels is.

Conclusions

We have investigated HBr and HCl oxidation on rutile RuO_2, IrO_2, and TiO_2 catalysts by applying an integrated approach consisting of advanced methods to analyse and compare their surface chemistry. We found that the structural stability of HX oxidation catalysts depends on the interaction of the hydrogen halide molecule with the catalyst surface. The combined HRTEM, DFT, and TAP study reveal that the amorphisation of the RuO_2 particle surface after treatment with HBr is due to structural distortion of the clean surface geometry after extensive bromination. Notice however that strong bromination and thus surface amorphisation occurred also in HBr oxidation. The impact of HCl is much more limited, leading to less pronounced distortion as a result of the comparably unfavourable energetics of oxygen substitution, restricting the Cl replacement to the surface. The computed bromine substitution into the TiO_2 lattice is endothermic, suggesting only limited potential for bromination. The TAP experiments support these results, indicating a stronger interaction of rutile-type materials with HBr than HCl. Further pulsing experiments in TAP indicate that halogen evolution can be considered to be the most energy-demanding step, with the activity of the catalysts for HBr oxidation increasing in the following order; $IrO_2 < TiO_2 < RuO_2$. This coincides with the computational results. Both reaction of HBr and HCl oxidation follow a Langmuir-Hinshelwood type mechanism on surfaces with a low to moderate degree of halogenation, as confirmed through pump-probe experiments. The halogen uptake is the key descriptor linking stability and activity of the catalytic systems. On RuO_2 the steady-state surface halogen coverage reaches 86-100% for chlorine and 75-300% for bromine, proving that subsurface bromination occurs, agreeing with the HRTEM and DFT studies. A decrease in the halogen coverage on RuO_2 can be induced by increasing the operation temperature and elevating the O_2:HX feed ratios. Still, our tools cannot describe in detail the mechanism for surface brominations. It is possible that some degree of subsurface Br uptake takes place early during the reaction process before the surface is completely saturated with bromine. This will affect the catalyst activity in the long term, even at higher temperatures. In contrast, the halogen coverage of TiO_2 is limited to 30-50% as a result of its self-doping mechanism with bromine. An increase in the temperature and the O_2:HX feed ratio induces higher activity, but does not significantly affect the halogen coverage on TiO_2. The addition of Br_2 to the gas feed over TiO_2 does not affect the bromine coverage, but inhibits the reaction at an apparent order of −0.44, indicating a competitive adsorption of Br_2 and HBr on the active sites. As a result of this study, we consider it highly desirable to combine the exceptional low-temperature activity of RuO_2 with the stability of TiO_2 against strong surface halogenation by designing new Ru-Ti mixed oxide catalysts for HBr oxidation with an optimal balance between activity and stability.

Acknowledgements

We thank Dr. Frank Krumeich and ScopeM, the Scientific Center for Optical and Electron Microscopy of ETH Zurich, for microscopic studies and the BSC-RES for providing computational resources. The Swiss National Science Foundation (SNF project number 200021-156107), the European Union's 7th Framework Programme (NMI3-II grant number 283883), the ICIQ Foundation, and the MINECO (Grant number CTQ2012-33826/BQU) are acknowledged for financial support.

Notes and references

‡ The *ab initio* thermodynamics should be interpreted with caution as a number of approximations (*i.e.* configurational entropies are missing) have been implicitly included, and thus this model only serves for qualitative purposes.

§ The preference for bromination can be seen from the fact that the transition between 2A and 4B configurations occurs at lower pressures than for Cl.

§§ For TiO_2, two different configurations were tested and the most stable one is taken into accounted for.

1 (a) J. Pérez-Ramírez, C. Mondelli, T. Schmidt, O. F.-K. Schlüter, A. Wolf, L. Mleczko, T. Dreier, *Energy Environ. Sci.*, 2011, **4**, 4786; (b) H. Over, *Chem. Rev.*, 2012, **112**, 3356.
2 (a) A. Fujishima, X. T. Zhang, D. A. Tryk, *Surf. Sci. Rep.,* 2008, **63**, 515; (b) Y. Lee, J. Suntivich, K. J. May, E. E. Perry, Y. Shao-Horn, *J. Phys Chem. Lett.,* 2012, **3**, 399.
3 (a) K. Seki, *Catal. Surv. Asia*, 2010, **14**, 168; (b) A. P. Amrute, C. Mondelli, T. Schmidt, R. Hauert, J. Pérez-Ramírez, *ChemCatChem*, 2013, **5**, 748.
4 (a) N. López, J. Gómez-Segura, R. P. Marín, J. Pérez-Ramírez, *J. Catal.,* 2008, **255**, 29; (b) D. Crihan, M. Knapp, S. Zweidinger, E. Lundgren, C. J. Weststrate, J. N. Andersen, A. P. Seitsonen, H. Over, *Angew. Chem., Int. Ed.,* 2008, **47**, 2131; (c) A. P. Seitsonen, H. Over, *J. Phys. Chem. C,* 2010, **114**, 22624; (d) M. G. Hevia, A. P. Amrute, T. Schmidt, J. Pérez-Ramírez, *J. Catal.*, 2010, **276**, 141.
5 (a) D. Teschner, R. Farra, L. Yao, R. Schlögl, H. Soerijanto, R. Schomäcker, T. Schmidt, L. Szentmiklósi, A. P. Amrute, C. Mondelli, J. Pérez-Ramírez, G. Novell-Leruth, N. López, *J. Catal.*, 2012, **285**, 273; (b) D. Teschner, G. Novell-Leruth, R. Farra, A. Knop-Gericke, R. Schlögl, L. Szentmiklósi, M. G. Hevia, H. Soerijanto, R. Schomäcker, J. Pérez-Ramírez, N. López, *Nat. Chem.*, 2012, **4**, 739.
6 (a) E. McFarland, *Science,* 2012, **338**, 340; (b) A. Toftelund, I. C. Man, H. A. Hansen, F. Abild-Pedersen, T. Bligaard, J. Rossmeisl, F. Studt, *ChemCatChem*, 2012, **4**, 1856; (c) K. Ding, H. Metiu, G. D. Stucky, *ChemCatChem*, 2013, **5**, 1906; (d) M. Moser, L. Rodríguez-García, A. P. Amrute, J. Pérez-Ramírez, *ChemCatChem*, 2013, **5**, 3520.
7 M. Moser, I. Czekaj, N. López, J. Pérez-Ramírez, *Angew. Chem., Int. Ed.*, 2014, **53**, 8628.
8 (a) G. Kresse, J. Furthmüller, *Comput. Mater. Sci.*, 1996, **6**, 15; (b) G. Kresse, J. Furthmüller, *Phys. Rev. B,* 1996, **54**, 11169.
9 H. Monkhorst, J. Pack, *Phys. Rev. B*, 1976, **13**, 5188.
10 J. P. Perdew, K. Burke, M. Ernzerhof, *Phys. Rev. Lett.*, 1996, **77**, 3865.
11 (a) M. Cococcioni, S. de Gironcoli, *Phys. Rev. B*, 2005, **71**, 035105, 1; (b) H. J. Kulik, M. Cococcioni, D. A. Scherlis, N. Marzari, *Phys. Rev. Lett.*, 2006, **97**, 103001, 1.
12 P. E. Blöchl, *Phys. Rev. B*, 1994, **50**, 17953.
13 G. Henkelman, B. P. Uberuaga, H. J. Jónsson, *Chem. Phys.*, 2000, **113**, 9901.
14 NIST, http://webbook.nist.gov/chemistry, (8th July 2015).
15 (a) J. T. Gleaves, G. S. Yablonsky, P. Phanawadee, Y. Schuurman, *Appl. Catal., A*, 1997, **160**, 55; (b) S. O. Shekhtman, G. S. Yablonsky, S. Chen, J. T. Gleaves, *Chem. Eng. Sci.*, 1999, **54**, 4371; (c) J. Pérez-Ramírez, E. V. Kondratenko, *Catal. Today*, 2007, **121**, 160; (d) J. T. Gleaves, G. S. Yablonsky, X. Zheng, R. Fushimi, P. L. Mills, *J. Mol. Catal. A: Chem.*, 2010, **315**, 108.
16 R. Farra, M. Eichelbaum, R. Schlögl, L. Szentmiklósi, T. Schmidt, A. P. Amrute, C. Mondelli, J. Pérez-Ramírez, D. Teschner, *J. Catal.*, 2013, **297**, 119.
17 G. Novell-Leruth, G. Carchini, N. López, *J. Chem. Phys.,* 2013, **138**, 1947061.
18 A. P. Amrute, C. Mondelli, M. A. G. Hevia, J. Pérez-Ramírez, *J. Phys. Chem C*, 2011, **115**, 1056.
19 M. Moser, C. Mondelli, A. P. Amrute, A. Tazawa, D. Teschner, M. E. Schuster, A. Klein-Hoffman, N. López, T. Schmidt, J. Pérez-Ramírez, *ACS Catal.,* 2013, **3**, 2813.
20 B. Li, H. Metiu, *J. Phys. Chem. C*, 2012, **116**, 4137.
21 Z. Révay, T. Belgya, *Principles of the PGAA method* in *Handbook of Prompt Gamma Activation Analysis with Neutron Beams*, ed. G. L. Molnár, Kluwer, 2004, Sections 3.2-3.3, pp. 23–28.
22 Z. Zhang, J. T. Yates, *Chem. Rev.*, 2012, **112**, 5520.